Measuring Retinal Fluorescein Leakage into the Human Vitreous with a Modified Confocal Scanning Laser Ophthalmoscope

Rui C. Bernardes, BSc., Conceição L. Lobo, MD, MSc., José G. Cunha-Vaz, MD, Ph.D.

Resumo – Descreve-se neste trabalho um método de quantificação de um índice de permeabilidade da barreira hemato-retiniana para a fluoresceína. Os dados são obtidos no vítreo do olho humano em tempos diferentes após administração intravenosa de fluoresceína por um sistema confocal de varrimento laser modificado. O processamento inclui o aumento de contraste da imagem do fundo ocular, alinhamento de imagens, construção, filtragem e interpolação de perfis, ajuste exponencial e integração. A determinação automática do centro da fovea é obtida por um processo de correlação cruzada. Uma grelha é sobreposta na imagem da retina e no mapa de índices de permeabilidade, o que permite uma mais fácil correlação entre as estruturas da retina e as alterações da permeabilidade da barreira hemato-retiniana para a fluoresceína.

Abstract - A method is described to quantify blood-retinal barrier permeability to fluorescein. Data are collected from the vitreous of the human eye at two elapsed time intervals after intravenous fluorescein administration, using a modified confocal scanning laser ophthalmoscope. Data processing includes fundus image enhancement, image alignment, profile construction, filtering and interpolation, exponential fit and integration. Automatic determination of the center of fovea is obtained by a cross-correlation process. Grid overlapping on fundus images and on permeability maps allows for matching chorioretinal morphological structures with alterations of blood-retinal barrier permeability to fluorescein.

I. INTRODUCTION

Alterations of the blood-retinal barrier (BRB) are associated with the development and progression of most retinal vascular diseases, many of them leading to important visual loss.

The diagnostic instrumentation presently available, fluorescein angiography and vitreous fluorometry, identify and measure this alteration of BRB as an abnormal leakage of fluorescein, but are unable to precisely quantify the individual sites of alteration.

We have been able to measure localized alterations of the BRB and map their location by modifying a prototype Zeiss confocal scanning laser ophthalmoscope. The instrument here described is known as Retinal Leakage Analyzer (RLA).

Having two compartments with different concentrations of fluorescein and a barrier with a given permeability between them, the movement of fluorescein from the higher to the lower concentration compartment will depend on the difference between concentrations and on the permeability of the barrier to fluorescein.

If we trace a profile of concentration in a normal direction to the barrier and considering its width as zero, we will have a step function (in a time prior to any movement of fluorescein between the two compartments).

For an eye, the first compartment will be the vessels, the barrier will be the BRB and the second compartment will be the vitreous.

To measure the BRB permeability to fluorescein, an intravenous administration of fluorescein is given to the patient under analysis.

Taking a first scan shortly after the administration of fluorescein to the patient and a second scan 30 minutes after the administration will allow to produce two profiles of concentration of fluorescein. The difference between these two profiles, after correcting for the decay of fluorescein in the plasma along the time interval between the first and second scan, will indicate the distribution of concentration of fluorescein inside the vitreous, whose integral indicates the amount of fluorescein in the vitreous in front of the measuring point. Normalizing this integral with the integral of free plasma fluorescein gives an index of permeability of the BRB to fluorescein.

This method constitutes a completely new approach and is the first one to allow for the localized measure of BRB permeability to fluorescein. It also allows the early detection of changes in the BRB even before any detectable changes in the fundus image, which constitutes an important step in the detection and understanding of the diabetic retinopathy disease.

II. MATERIAL AND METHODS

A Zeiss prototype confocal scanning laser ophthalmoscope was modified to obtain fluorometric measurements in confocal optical planes across the retina and cortical vitreous.

Data were gathered with a modified Zeiss prototype confocal scanning laser ophthalmoscope in a volume of 3150 by 2700 by 2550 µm.

The instrumentation used has an *x* and *y* precision between 10 and 20 µm and an axial precision of 50 µm. For the current application it uses an argon laser of 488 nm with a power of 400 µW at the eye.

Data are gathered from 9 confocal planes with the confocal plane being continuously moved during the acquisition and an interlaced video signal is generated. This video signal can be directly shown in a video monitor and/or saved in a normal video tape recorder.

These features, interlaced video signal and continuous movement of the confocal plane during the acquisition, allow the separations of even an odd lines of the image since they belong to two different planes.

This way, each scan is made by 18 images from 18 confocal planes along 2550 µm, with the confocal plane being continuously moved during acquisition. The tile effect presents no problems due to the type of profile processing that will be done.

Several changes were introduced in the original system: photomultiplier gain; offset; barrier filter; automatic focus; and acquisition software.

In order to be able to convert light intensity to fluorescein concentration the gain of the photomultiplier tube has to be kept constant along the acquisition. To achieve this objective the feedback signal has been interrupted and a fixed gain chosen. After calibration using a set of cuvettes with a known fluorescein concentration, we are able to convert light intensity to equivalent fluorescein concentration.

The offset of the image is kept constant to allow for the conversion and was made equal to zero to increase the dynamic range of the signal.

To improve reproducibility and easy of use, the start signal has been interrupted and a new hardware circuit introduced. After the user has focused in the retina of the patient, he presses the start knob. The new introduced circuit receives this signal and moves the confocal plane to a new location posterior to the retina. It also turns the barrier filter on, selects the correct confocal aperture and initiates the normal acquisition process.

Initially the barrier filter is off to allow the collection of fluorescent light and reflectance of the excitation light. To quantify the concentration of fluorescein in the vitreous the reflection component has to be blocked and only the fluorescent light is allowed to reach the photomultiplier tube. The barrier filter is a low-pass filter with high attenuation for the 488 nm and low attenuation for the range 520 to 630 nm.

After acquisition the barrier filter is turned off to allow for the next focus on the patient retina. All these steps are done with signals generated with the introduced circuit.

Fundamental aspects of the system as calibration, lower limit of detection, accuracy and reproducibility, are discussed elsewere.[1]

All the processes, but the increase in the sampling rate and image interpolation, which are already implemented in the toolboxes, have been implemented in Matlab using the Signal and Image Processing Toolboxes.

Two scans are necessary to compute and build a map of permeability index of the BRB to fluorescein, the first taken before 5' have elapsed after intravenous fluorescein administration and the later taken at 30' after fluorescein administration. Only the common part of both scans is processed. To achieve this objective for each scan an integration process followed by a contrast enhancement builds a fundus image.
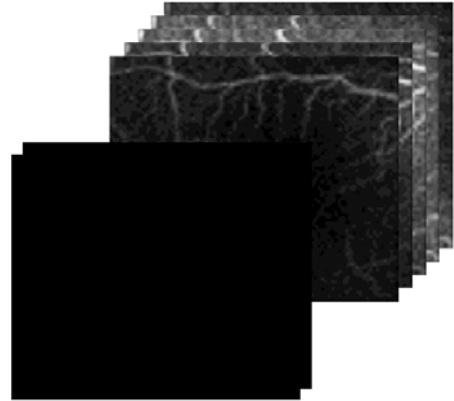

Fig. 1 - Gathered confocal planes.

The fundus image has to be built by an integration process because images are tiled, i.e., none of those confocal planes shown in the previous figure correspond to the retina plane. Also shown in the previous figure is the fact that the anterior images, which correspond to acquisitions made in the vitreous, do not contain any morphological information. This means that they should not be included in the process of integration.

Considering these facts, we have only considered the four images near to the retina, which have the higher mean values, to be summed into a new image.

This new image is then converted to the original 256 levels (1 byte) and to increase contrast the conversion is made non-linear.

The following two images show the result of a linear conversion and the result of the non-linear conversion.
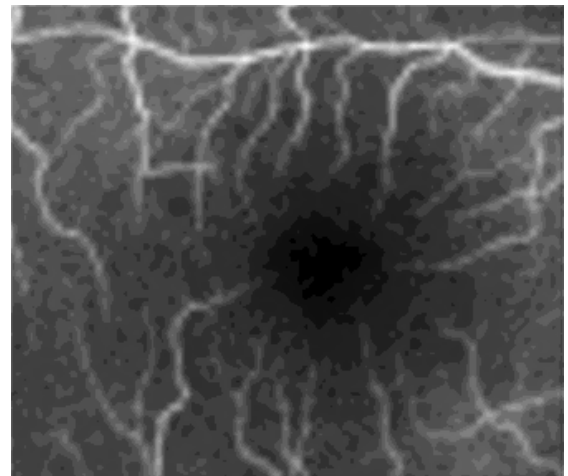

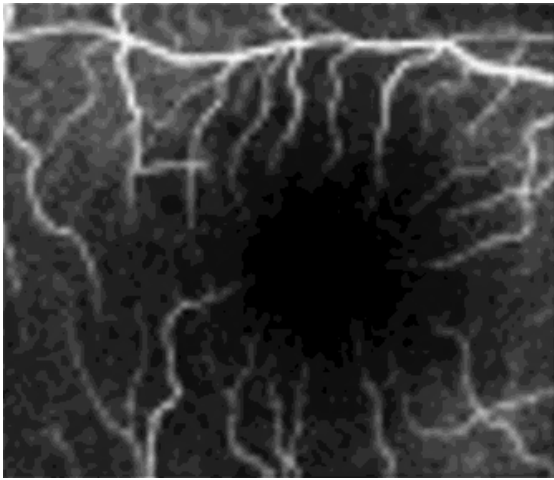Fig. 2 - Result of a linear factor.

Fig. 3 - Result of a non-linear factor.

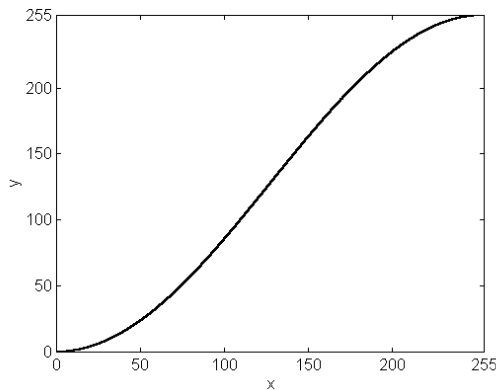The non-linear factor is shown in the next figure.

Fig. 4 – Graph of the non-linear factor used.

Another important aspect is the fact that the gathered data are not as detailed as shown in the previous images. Due to the separation of the even and odd lines, we have to compute mean values in relative large areas (8 x 4 pixels). For processing purposes we only have 84 by 72 pixels. The corresponding image is as show in the next figure.
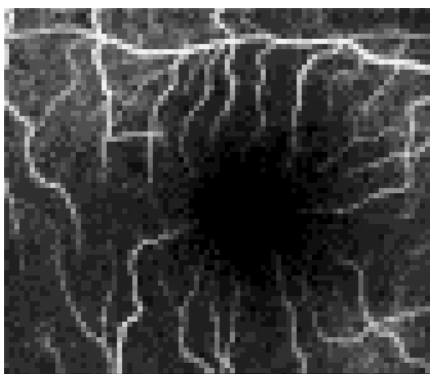

Fig. 5 - 84 by 72 pixel image.

This image is then interpolated by a bicubic method and the result is as shown in figure 3, where the fundus image appears more natural. The chosen factor for interpolation

is 4 and the interpolated image is only to presentation purposes, any processing is always done over the gathered data.

After building the two fundus images, for the 5 and 30 minutes acquisitions, both images are aligned by an automatic process know as "Phase Correlation Process"[2].

This process is based in the shift property of the Fourier transform.

Being the transform of two images $g_1(x,y)$ and $g_2(x,y)$ the functions $G_1(u,v)$ and $G_2(u,v)$, respectively, both can be expressed in the Euler notation as:

$G_1(u,v) = e^{j\theta_1(u,v)}.|G_1(u,v)|$ and $G_2(u,v) = e^{j\theta_2(u,v)}.|G_2(u,v)|$.

Been θ_1 and θ_2 function of u and v, the conjugate of G_2 is $G_2^*(u,v) = e^{-j\theta_2(u,v)}.|G_2(u,v)|$, since $|G_2(u,v)| = |G_2^*(u,v)|$.

The product $G_1G_2^*$ written in a simplified notation is given by $G_1G_2^* = e^{j(\theta_1-\theta_2)}.|G_1|.|G_2^*|$.

That gives, $e^{j\theta} = G_1G_2^*/|G_1.G_2^*|$.

The shift in the image is then given by $\mathfrak{I}^{-1}\{e^{j\theta}\}$, i.e., $d(x,y) = \mathfrak{I}^{-1}\{ G_1G_2^*/|G_1.G_2^*|\}$.

This method is insensitive to differences in illumination and noise with a spectral density near to the spectral density of the images being processed. The former is a key aspect since it is a common problem in the collection of light from the eye fundus.

After image alignment, only the common portion of both scans is considered for further processing.

The following two figures show the result of the alignment process. The first image shows the fundus image for the first scan (5 minutes scan) with a point signaled by the user.

The second image shows the same eye fundus for the later scan (30 minutes scan) where it can be seen the result of the incoming of fluorescein into the vitreous with the fundus image less detailed. Nevertheless, the automatic signaled point is clearly the same one chosen by the user in the first image. This shows the performance of the alignment process in the application environment.
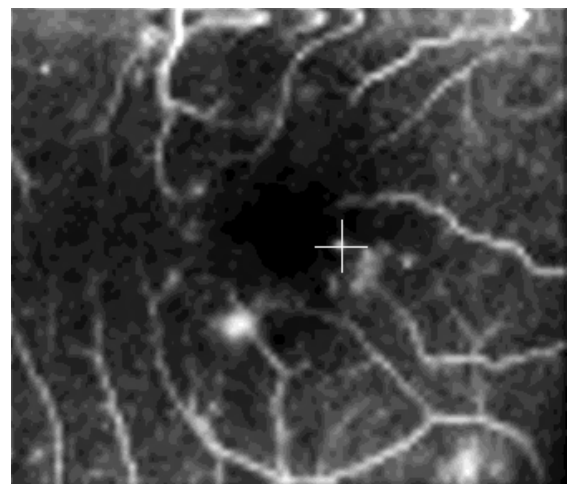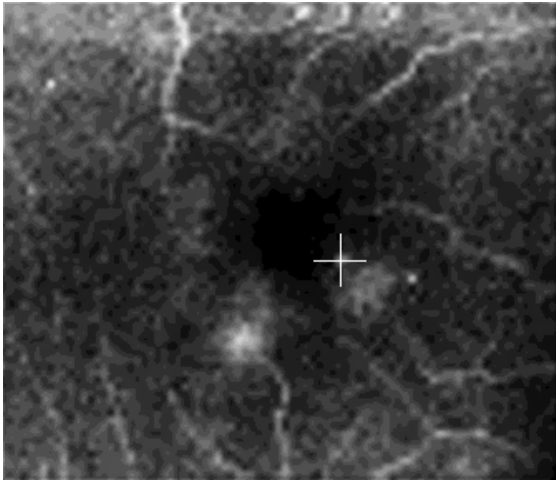

Fig. 6 – 5 minutes fundus image.

Fig. 7 – 30 minutes fundus image.

For each area of 2 by 2 pixels of the common part of both scans, a profile is built.

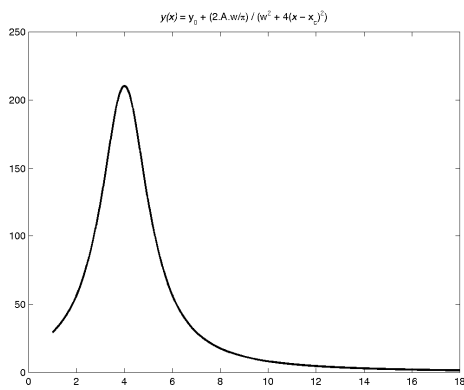The response of the system is a Laurentzian, as shown in the graph of the next figure.

$$y(x) = y_0 + (2.A.w/\pi) / (w^2 + 4(x - x_c)^2)$$

Fig. 8 – System response.

The distance of resolution, with the confocal aperture used for this work is 343 µm.

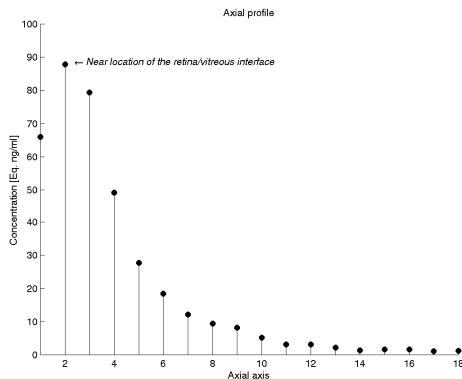The following figure shows a typical profile with 18 samples equally spaced.

Fig. 9- Profile before interpolation.

To improve reliability, an interpolation is performed for each profile[3].

The result of interpolation allows for an improved location of the retina/vitreous interface as shown in the next figure.
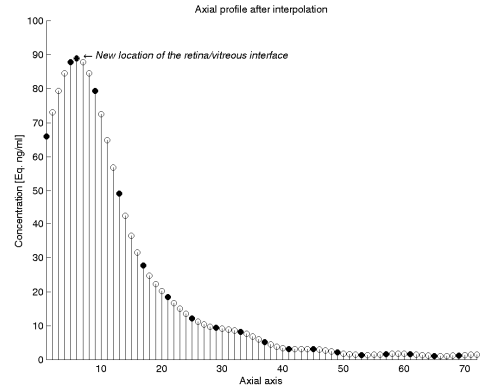
Fig. 10 – Profile after interpolation.

This profile shows a better approach for the location of the retina/vitreous interface and for the corresponding concentration value.

The difference in profiles gathered at less than 5 and 30 minutes after fluorescein administration, for the same area, is due to the incoming fluorescein across the blood-retinal barrier into the vitreous through that area.

To compute the difference, one profile has to be shifted until both locations of the retina/vitreous interface superimpose and the profile of the first acquisition has to be scaled down to the maximum value of the second profile, due to biological elimination of the fluorescein in the blood. Fluorescein is eliminated by the kidneys and converted in fluorescein monoglucoronate by the liver.

The fluorescence of monoglucoronate fluorescein can be neglected in the first hours and will not be considered in our processing since the later scan is taken 30 minutes after fluorescein administration.

Since the movement of the fluorescein in the vitreous is due to a diffusion process, a decay exponential is expected to be found from the retina/vitreous interface into the vitreous.

The computed difference between profiles starts at zero, increases until reaches a maximum and then decreases as a decay exponential.

A decay exponential is fitted to the difference between profiles after the maximum as been reached.

A typical fit is shown in the next figure in a logarithmic scale.
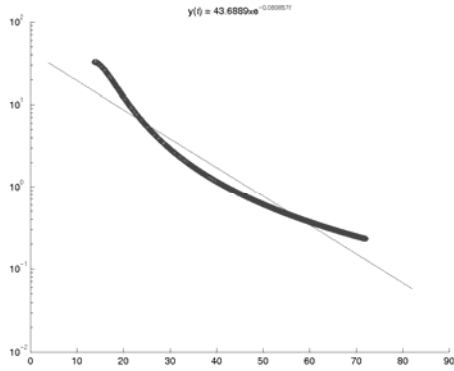
Fig. 11 – Exponential fit.

The integral of this exponential divided by the integral of free plasma fluorescein gives the permeability index for this area. Processing all areas, we are able to build a complete map.

Since data acquisition and fundus imaging are simultaneously done, there is a direct correlation between the computed map of permeability index and the morphology of the retina shown in the fundus image.

In order to facilitate the match of locations between the map of permeability index and the fundus image, the center of the fovea is automatically determined and signaled and a grid is superimposed in the fundus image and in the map. Also, two concentric circles are shown centered in the fovea, one with 100 µm and another with 750 µm.

To determine the center of the fovea, the fundus image is compressed with a logarithmic function to increase the difference between vascular and avascular zones.

A normal fundus image is shown in the next figure.
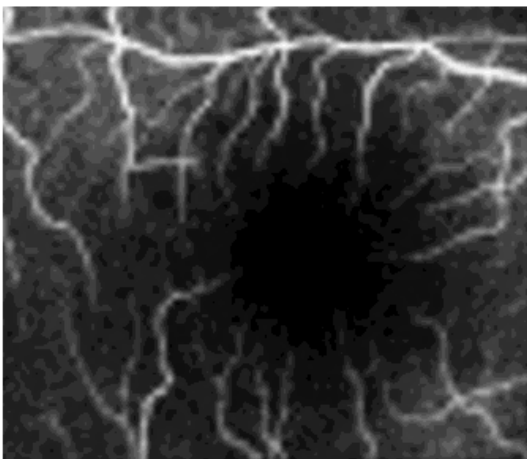

Fig. 12 – normal fundus image.

The same eye fundus is shown on the next image after compression.
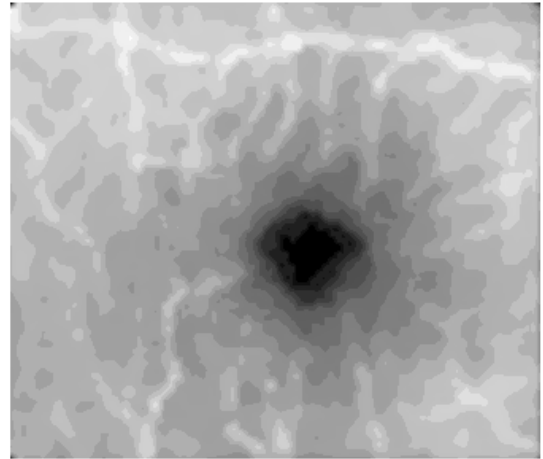

Fig. 13 – fundus image after LOG compression.

To have the central area, i.e., the fovea, with higher values, we have to work with the negative of this new image, as can be seen in 3D in the next figure, where the plotted data have been smoothed with a median filter to remove isolated peaks. It is clearly seen that there is a difference between the vascular and avascular zones.
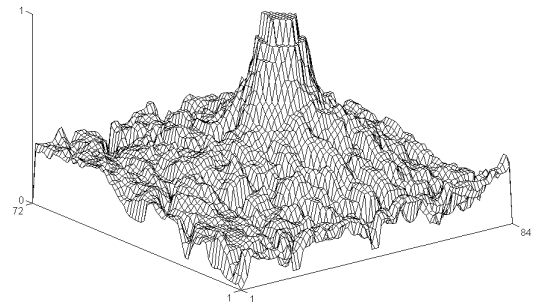

Fig. 14 – Compressed image plotted in 3D.

The maximum value of the cross-correlation function is shown as one since this value is not important, only its location.

A cross-correlation is then computed between the resulting image and a 3D Gaussian function, having the center of the Gaussian in the center of the image.

The parameters of the Gaussian function have to be chosen carefully.

For the full-width at half-weight parameter we have to consider that if we have chosen a small value we will find several peaks in the correlation and if we chose a large value we have to take into consideration values of the compressed image that do not make part of the central area.

Also the limits of the Gaussian function should be chosen considering that Matlab append zeros to the smaller of the two signals before computing the correlation. In this way, there is no advantage to define the Gaussian smaller nor larger than the size of the image, since costs in terms of computation are the same. Also, if the size of the image differs from the size of the Gaussian

this fact has to be taken into account when looking for the shift of the maximum of the correlation regarding the center of the foveal avascular zone.

Having the Gaussian with the same size of the image, the shift of the maximum value of the correlation to its center is equal to the shift of the center of the fovea to the center of the eye fundus image.

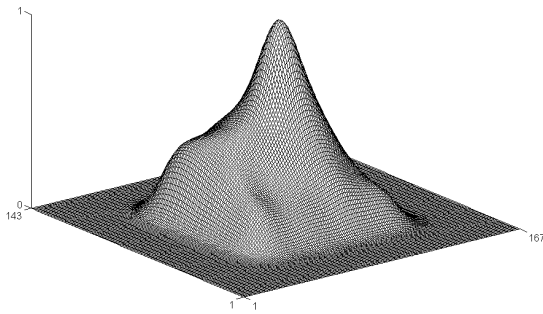The correlation function is plotted in the graph of the next figure.

Fig. 15 – Correlation function.

The result of this process is as shown in the next figure.
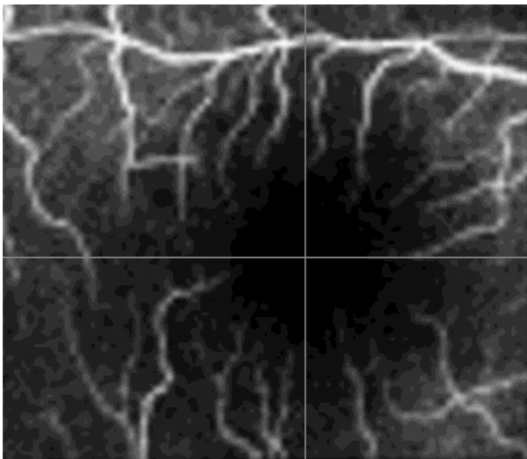
Fig. 16 – Fundus image with the center of the fovea signaled.

This process is relatively immune to light collection problems into the extent of acceptance for the remaining processing.

The following figure shows a fundus image where the presence of a shaded area does not affect the determination of the center of the fovea.
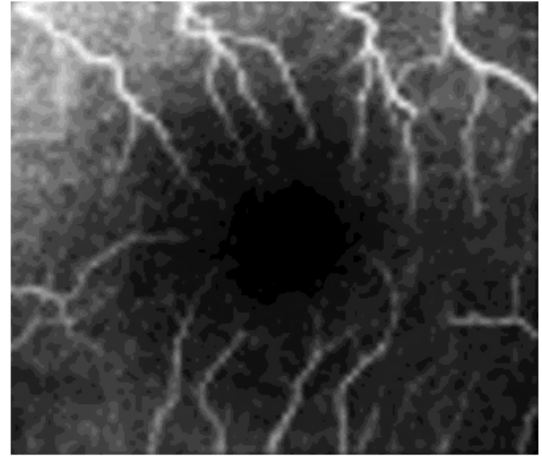

Fig. 17 – Fundus image.

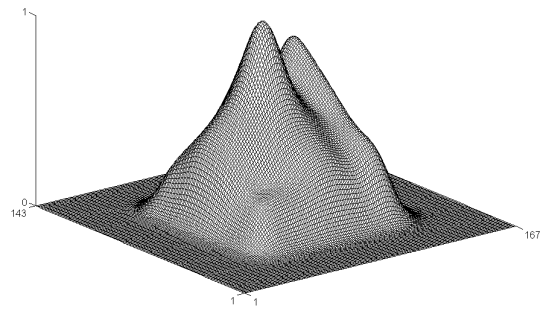The graph of the correlation function for this image is plotted in the next figure.

Fig. 18 – Two distinct peaks in the correlation function.

In this case the presence of the second peak is due to the collection of light but the process produces the correct determination as it can be seen in the next figure.
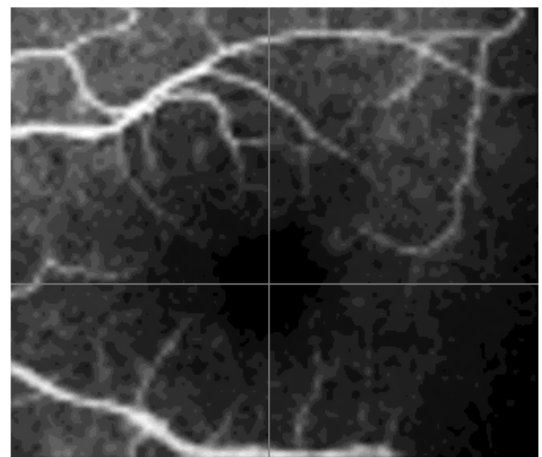

Fig. 19 – Correct determination of the center of the fovea.

For extreme cases, as in the *"drusen"* eyes, the process is unable to determine the correct location of the center of the fovea due to the hyperfluorescence of the retina independently of morphology. This case is reported in the following two figures.
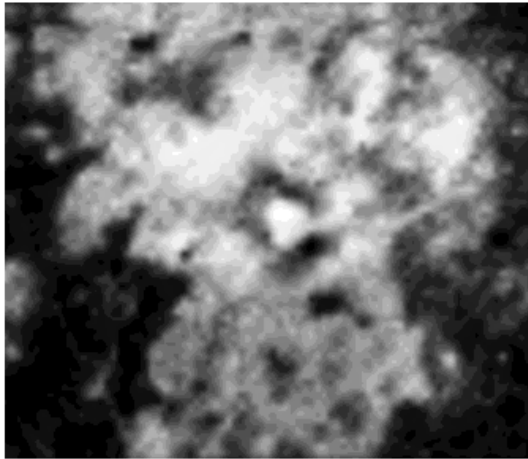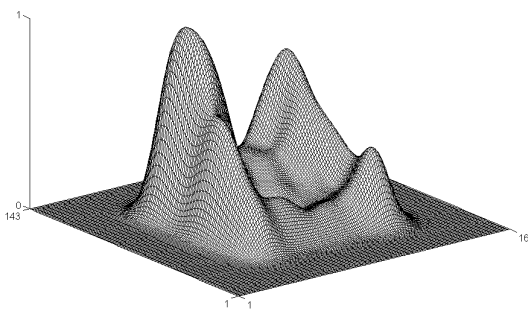
Fig. 20 – Drusen retina.

Fig. 21 – Correlation .

Finally, the results of these processes are shown in the next two figures, the fundus image and the RLA map, respectively.
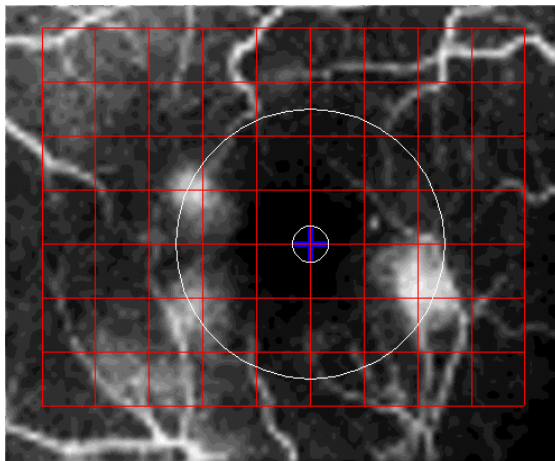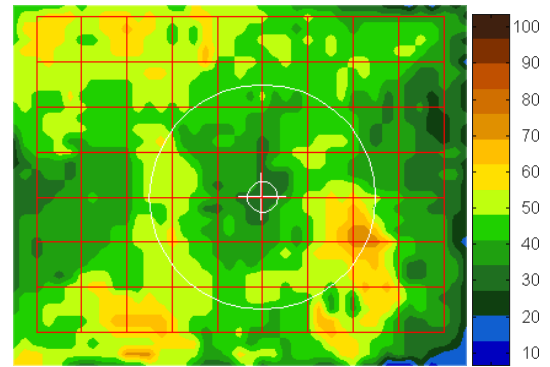

Fig. 22 – Fundus image.

Fig. 23 – Rlmap. Units are x 10^{-7} cm/s

III. RESULTS

A map of permeability index of the BRB barrier to fluorescein and a fundus image are built from the gathered data. The map is represented in a false color code and units are cm/sec.

A grid is overlapped on the map as well as on the fundus image, with a grid spacing of 300 µm.

Two concentric circles are also plot, centered on the fovea and with radius of 100 and 750 µm. Lateral resolution of the map is in the order of 75-100 µm.

IV. CONCLUSION

The method here described allows the localization and measurement of the alterations of the BRB that occur in human retinal disease, on a clinical setting and represents a promising step in the follow-up and early diagnosis of retinal vascular diseases. A major advantage of the system is its ability to simultaneously image the retina, allowing the correlation between the maps of BRB permeability and any changes occurring in retinal anatomy. This also allows for the integration with other systems like the "Retinal Thickness Analyzer" or "Optical Coherence Tomography". That integration offers the way for multimodal imaging of the eye fundus, offers the physician a new perspective of the retinal disease and improves the understanding and evaluation of the disease.

REFERENCES

[1] C.L. Lobo, R.C. Bernardes, F.J. Santos and J.G. Cunha-Vaz, "Mapping Retinal Fluorescein Leakage with Confocal Scanning Laser Fluorometry of the Human Vitreous". Arch Ophthalmol. 1999, 117:631-637

[2] J. J. Pearson, D. C. Hines, Jr, S. Golosman and C. D. Kuglin "Video-Rate Image Correlation Processor", Applications of Digital Image Processing. Proceedings of the International Optical Computing Conference '77, SPIE Volume 119, page 197.

[3] IEEE. Programs for Digital Signal Processing. IEEE Press. New York: John Wiley & Sons, 1979. Algorithm 8.1